Clim. Past, 7, 235–247, 2011
www.clim-past.net/7/235/2011/
doi:10.5194/cp-7-235-2011

Climate of the Past

A new mechanism for the two-step δ^{18}O signal at the Eocene-Oligocene boundary

M. Tigchelaar[1,*], **A. S. von der Heydt**[1], **and H. A. Dijkstra**[1]

[1]Institute for Marine and Atmospheric Research Utrecht, Utrecht University, Utrecht, The Netherlands
[*]current at: School of Ocean and Earth Science and Technology, University of Hawaii at Mānoa, Honolulu, Hawaii, USA

Received: 2 July 2010 – Published in Clim. Past Discuss.: 21 July 2010
Revised: 25 January 2011 – Accepted: 7 February 2011 – Published: 9 March 2011

Abstract. The most marked step in the global climate transition from "Greenhouse" to "Icehouse" Earth occurred at the Eocene-Oligocene (E-O) boundary, 33.7 Ma. Evidence for climatic changes comes from many sources, including the marine benthic δ^{18}O record, showing an increase by 1.2–1.5‰ at this time. This positive excursion is characterised by two steps, separated by a plateau. The increase in δ^{18}O values has been attributed to rapid glaciation of the Antarctic continent, previously ice-free. Simultaneous changes in the δ^{13}C record are suggestive of a greenhouse gas control on climate. Previous modelling studies show that a decline in pCO_2 beyond a certain threshold value may have initiated the growth of a Southern Hemispheric ice sheet. These studies were not able to conclusively explain the remarkable two-step profile in δ^{18}O. Furthermore, they considered changes in the ocean circulation only regionally, or indirectly through the oceanic heat transport. The potential role of global changes in ocean circulation in the E-O transition has not been addressed yet. Here a new interpretation of the δ^{18}O signal is presented, based on model simulations using a simple coupled 8-box-ocean, 4-box-atmosphere model with an added land ice component. The model was forced with a slowly decreasing atmospheric carbon dioxide concentration. It is argued that the first step in the δ^{18}O record reflects a shift in meridional overturning circulation from a Southern Ocean to a bipolar source of deep-water formation, which is associated with a cooling of the deep sea. The second step in the δ^{18}O profile occurs due to a rapid glaciation of the Antarctic continent. This new mechanism is a robust outcome of our model and is qualitatively in close agreement with proxy data.

Correspondence to: M. Tigchelaar
(mtigch@hawaii.edu)

1 Introduction

While the long-term variations in our present-day climate are paced by the waxing and waning of the Northern Hemispheric ice sheet, Earth's surface was (almost) entirely ice-free at the beginning of the Cenozoic Era, 65.5 Ma. In the course of this Era, Earth's climate experienced a transition from a "Greenhouse" world to the current "Icehouse" world, the most marked step of which occurred close to the Eocene-Oligocene (E-O) boundary, 33.7 Ma. The Eocene climate was relatively warm, with polar surface and deep water temperatures up to 10 °C warmer than today. The Antarctic continent – though in its present position – was ice-free and lushly vegetated. At the E-O boundary, global temperatures dropped and a semi-permanent ice-sheet formed on Antarctica. An overwhelming amount of evidence from fossils and proxies indicates that climate change at the E-O boundary was global and involved all parts of the climate system (Lear et al., 2000; DeConto and Pollard, 2003a; Dockery and Lozouet, 2003; Hay et al., 2005; Zachos and Kump, 2005; Coxall and Pearson, 2007; Liu et al., 2009).

The most pronounced evidence for relatively rapid climatic changes comes from the marine δ^{18}O record. Numerous cores taken from the ocean floor display an abrupt increase in δ^{18}O of 1.2–1.5‰ across the E-O boundary. The shift lasts approximately 500 kyr and is characterised by a remarkable two-step profile in which two 40-kyr steps are separated by a plateau of 200 kyr. The E-O transition terminates with a sustained maximum persisting for 400 kyr, followed by several stepped decreases (Coxall et al., 2005). Eventually δ^{18}O values stabilise ∼31 Ma to a value ∼1‰ higher than before the transition (Zachos et al., 1996; Zachos and Kump, 2005; Coxall and Pearson, 2007).

The rapid shift in δ^{18}O towards a sustained maximum has been associated with a rapid and extensive glaciation of at least the Antarctic continent. Glaciomarine sediments in the vicinity of the Antarctic continent support this interpretation.

Published by Copernicus Publications on behalf of the European Geosciences Union.

Although Northern Hemispheric ice rafted debris dating back to the middle Eocene has also been found, data are insufficient to determine the extent of a Northern Hemisphere glaciation at this time (Eldrett et al., 2007). It is highly likely that a rapid glaciation of the Antarctic continent was accompanied by a (local) decrease in temperature and there are many indications that the δ^{18}O signal comprises both an ice volume and a temperature change (Oerlemans, 2004; Coxall and Pearson, 2007; de Boer et al., 2010). Analysis of the Mg/Ca-ratio in benthic foraminifera indicates a cooling of up to 2.5 °C in the tropics (Lear et al., 2000, 2004, 2008). $U_{37}^{K'}$ and TEX_{86} analyses have lead to the conclusion that high-latitude sea surface temperatures (SSTs) decreased by 4.8–5.4 °C from the late Eocene to the early and mid-Oligocene. Model simulations show that such a decrease in SSTs corresponds to a decrease in deep-water temperatures of 3–5 °C. Combining this result with the δ^{18}O record produces maximum ice volume estimates of 40–120% of modern Antarctic ice volume (Liu et al., 2009).

Changes in the global carbon cycle are reflected in the δ^{13}C record, which displays a rapid and stepwise increase of 1‰ similar in shape and duration to the shift observed in δ^{18}O values. The increase in δ^{13}C is thought to be indicative of enhanced marine export production (Zachos and Kump, 2005; Coxall and Pearson, 2007). The sharp rise of carbon isotope ratios has also been associated with a two-step deepening of the carbon compensation depth (CCD) by more than 1 km (Rea and Lyle, 2005; Zachos and Kump, 2005). The CCD is linked to ocean acidity, which is in turn linked to atmospheric CO_2 concentration (Coxall et al., 2005; Merico et al., 2008). Proxy records show a general decline in pCO_2 throughout the Cenozoic from 2–5 times pre-industrial atmospheric levels (PAL) in the mid-Eocene, to near-modern values in the lower Miocene, although sufficient detail to accurately determine the CO_2 decline across the E-O boundary is lacking (Pagani et al., 2005; Coxall and Pearson, 2007; Pearson et al., 2009).

During the Eocene, the Southern Ocean and even mid-latitudes are thought to have played a greater role in deep-water formation. Sedimentary and seismic evidence in combination with analysis of neodymium (Nd) isotopes shows that there was a transition from a southern sinking source to a bipolar source of deep-water formation at the beginning of the Oligocene (Thomas et al., 2003; Thomas, 2004; Via and Thomas, 2006). The initiation of deep water formation in the North Atlantic was facilitated by the subsidence of the Greenland-Scotland Ridge which may have occurred around the E-O boundary (Davies et al., 2001). Other implied climatic changes include an increased latitudinal temperature gradient, more powerful atmospheric circulation, higher aridity and changes in seasonality (Coxall et al., 2005; Eldrett et al., 2009).

Currently two main hypotheses explaining the complex E-O climate transition abide; one involves the opening of ocean gateways around the E-O boundary, the other uses declining CO_2 values below a certain threshold value as the main driver. The opening of Drake Passage between Antarctica and South America and of Tasmanian Passage between Antarctica and Australia has facilitated the organisation of the Antarctic Circumpolar Current (ACC), reducing southward oceanic heat transport and cooling Southern Ocean SSTs. Since the opening of these passages occurred around the E-O boundary, it might have played a dominant role in the glaciation of Antarctica. Precise timing of the opening of these gateways has, however, proven to be problematic (Livermore et al., 2005; Scher and Martin, 2006; Coxall and Pearson, 2007). Evidence to support a vigourous ACC before the mid-Miocene is scarce (Coxall and Pearson, 2007). Furthermore, DeConto and Pollard (2003a) argue that the influence of colder Southern Ocean SSTs on Antarctic meteorology is poorly resolved, and Huber and Nof (2006) demonstrate that ocean heat transport would have had to decrease enormously for any significant changes in Antarctic continental temperatures to occur.

Huber and Nof (2006) argue additionally that the major changes in productivity during the E-O transition are strong evidence in favour of a greenhouse gas control on climate. It has been proposed that, once some CO_2 threshold (∼750 ppm, Pearson et al., 2009) was reached, feedbacks related to snow/ice-albedo and ice-sheet height/mass-balance could have initiated rapid ice-sheet growth (DeConto and Pollard, 2003a,b; Coxall and Pearson, 2007). DeConto and Pollard (2003a) ran a global climate model coupled to a dynamic ice-sheet model, forcing it with a CO_2 decline from 4 to 2 times PAL in 10 Myr. They found that relatively small ice caps form due to high levels of winter precipitation, which start to grow rapidly beyond some threshold CO_2 concentration and eventually coalesce to form one continental scale ice-sheet. In their simulations with a non-dynamical, 50-m slab ocean, the opening of Drake Passage only affects the timing of ice-sheet growth. Other modelling and data studies support the idea that the opening of Drake Passage and the subsequent development of the ACC may have helped ice growth on Antarctica but was not the ultimate cause (Sijp and England, 2004; Sijp et al., 2009; Cramer et al., 2009; Haywood et al., 2010). It is thought that the initiation and rapid growth of the ice-sheet is aided by the specific orbital settings at the E-O boundary: low eccentricity and low-amplitude changes in obliquity favour dampened seasonality and cold summers (DeConto and Pollard, 2003a,b; Coxall et al., 2005; Coxall and Pearson, 2007).

Thus far, model studies have largely focussed on the role of individual parts of the climate system. Since data show that climate change at the E-O boundary was global and involved all parts of the climate system, it is to be expected that interactions and feedbacks between the different climate system components are important. In addition, previous model studies have not addressed the potential role of changes in the ocean's meridional overturning circulation (MOC) in the E-O climate transition.

Table 1. Parameters that were changed from or added to Gildor et al. (2002).

Parameter, Unit	Description	Previous Value	New Value
$f_{L1},\ldots,f_{L4}$	land fraction	0.5, 0.2, 0.35, 0.5	0.21, 0.19, 0.30, 0.57
$K_{\text{h up}}$ [$\text{m}^2\,\text{s}^{-1}$]	surface horizontal diffusion coefficient	6.0×10^{-4}	1.5×10^{-4}
$K_{\text{h deep}}$ [$\text{m}^2\,\text{s}^{-1}$]	deep horizontal diffusion coefficient	7.5×10^{-3}	2.0×10^{-3}
K_{v} [$\text{m}\,\text{s}^{-1}$]	vertical mixing coefficient	7.0×10^{-8}	4.5×10^{-8}
r [s^{-1}]	friction coefficient	3.0×10^{-4}	4.2×10^{-8}
K_θ [$\text{s}^{-1}\,\text{K}^{-2}$]	atmospheric heat transport coefficient	15.5×10^{20}	13.5×10^{20}
$P_{lw1},\ldots,P_{lw4}$	atmospheric emissivity	0.61, 0.49, 0.52, 0.67	0.62, 0.53, 0.51, 0.70
$CO_{2\ \text{in}}$ [ppm]	pCO_2	320	1500
δ_{ice} [‰]	isotopic composition of ice		-35
${V_{\text{w}}}^0$ [m^3]	volume Eocene ocean		1.3×10^{18}
${\delta_{\text{w}}}^0$ [‰]	δ_{w} Eocene ocean		0.244
$IS_{\max}$ [m^3]	maximum volume Antarctic ice sheet	9×10^{16}	2.57×10^{16}

Here a new mechanism explaining the two δ^{18}O steps across the E-O transition record will be presented in which several parts of the climate system are involved and switches in the MOC play a dominant role. The transition from "Greenhouse" to "Icehouse" is simulated using an adapted version of the model developed by Gildor and Tziperman (2000, 2001) and Gildor et al. (2002). This model is a coupled 8-box-ocean, 4-box-atmosphere model with added land ice and sea ice components, the details of which will be briefly described in Sect. 2. In a model of such simplicity, the role and importance of the different mechanisms at work are (more) easily distinguishable.

In Sect. 3 it is argued that the first increase in δ^{18}O values represents (mostly) cooling of the deep sea. This cooling is brought about by a switch in the MOC from a southern sinking state to a bipolar sinking state. The second δ^{18}O step reflects the growth of the Antarctic ice sheet and further cooling as a result of this. The crucial control parameter inducing the two-step transition is the atmospheric carbon dioxide concentration. As will be shown in Sect. 4, our new mechanism is a robust outcome of the model and qualitatively in close agreement with proxy data.

2 The model

The model that is used is an adapted version of the coupled ocean-atmosphere-ice model that was developed by Gildor and Tziperman (2000, 2001) and Gildor et al. (2002) to explain the 100-kyr period observed in glacial-interglacial oscillations for the past 400 kyr. To this model we added a module to compute changes in δ^{18}O. By changing the parameters of the model, it can be adapted to paleoclimatic boundary conditions (see below). In this section the most important characteristics of the model are discussed; a full description of the equations can be found in Gildor and Tziperman (2001) and Gildor et al. (2002). An overview of the parameters that were altered with respect to Gildor et al. (2002) is presented in Table 1.

The ocean is represented by four surface boxes and four deep boxes whose latitudinal extends are South Pole to 45° S, 45° S to equator, equator to 45° N and 45° N to North Pole. The meridional overturning circulation is buoyancy driven; advection and diffusion of temperature and salinity are balanced by surface fluxes from the atmosphere and land ice components. The atmospheric model consists of four vertically averaged boxes representing the same latitude bands as the ocean boxes. The surface below the atmospheric boxes is a combination of ocean, land, land ice and sea ice, each with its specified albedo. The averaged potential temperature in the box is calculated on the basis of the energy balance in the box, consisting of: incoming solar radiation, using box albedo and with the possibility to include Milankovitch variations; outgoing long-wave radiation; heat-flux into the ocean; and meridional atmospheric heat transport. The meridional atmospheric moisture transport is proportional to the meridional temperature gradient and the humidity of the box to which the flux is directed. Precipitation is calculated as the convergence of the moisture fluxes.

The land ice model assumes a simple, zonally symmetric ice sheet of perfect plasticity. The ice sheet grows due to precipitation in the box, which is assumed to be distributed evenly. It decreases as a result of ablation, evaporation and calving processes. This sink term is taken to be constant in time, as it is expected that the source term dependence on temperature dominates that of the sink term (Ghil et al., 1987; Gildor and Tziperman, 2001). We set the maximum volume of the Antarctic ice sheet to its present-day value, $2.57\times10^{16}\,\text{m}^3$ (IPCC, 2007), to prevent it from growing beyond what the Antarctic continent is believed to be able to accommodate.

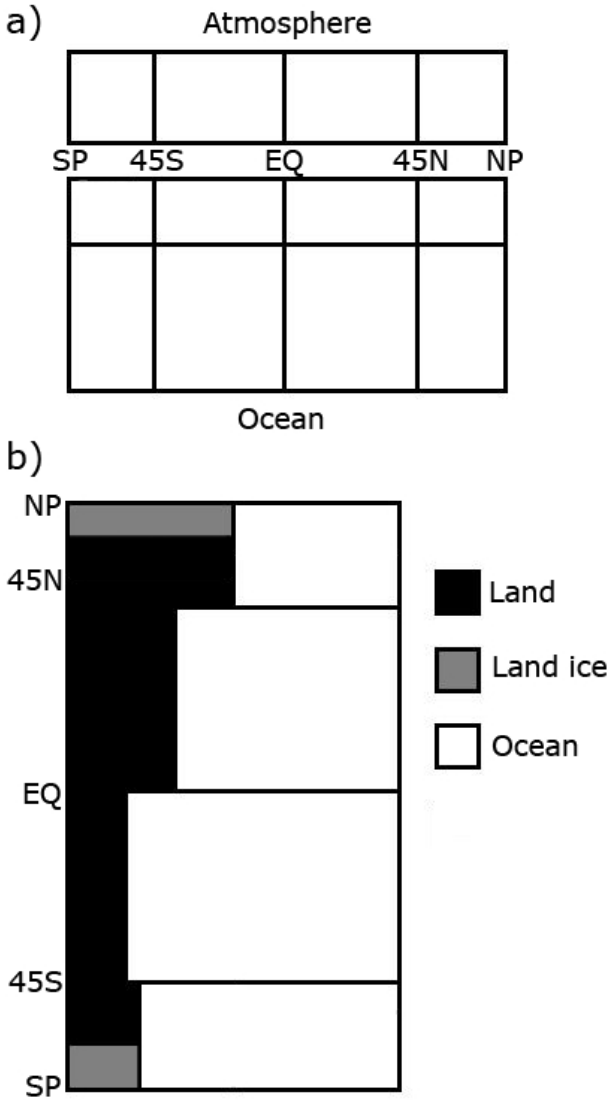

Fig. 1. Box model **(a)** meridional cross section **(b)** top view. Adapted from Gildor and Tziperman (2001).

A known problem of many models, including this one, is a too high sensitivity to the sea ice-albedo feedback. This means that when the ocean covers a large proportion of the box ($\geq$80%), the feedback mechanism will cause the ocean to be completely sea ice covered. Especially in the most southern box, where land fractions are low, this is problematic. Therefore – since there are no indications that sea ice changes played a dominant role in the Eocene-Oligocene transition (Huber and Sloan, 2001) – the sea ice component is left out of the study entirely to allow land fractions to take on realistic values. Hence, there will be no sea ice present in all boxes.

An additional module was added to the model that computes variations in δ^{18}O. The oxygen isotopic composition of sea-water δ_w is calculated using the volumetric changes in land ice and ocean and conservation of total δ^{18}O (Bintanja et al., 2005; de Boer et al., 2010):

$$V_w{}^0 \times \delta_w{}^0 = V_{ice} \times \delta_{ice} + V_w \times \delta_w \quad (1)$$

where $V_w{}^0$ is the volume of the Eocene ocean, and V_w is the volume of the ocean after ice formation: $V_w = V_w{}^0 - V_{ice}$. δ_{ice} is the isotopic composition of land ice and $\delta_w{}^0$ and δ_w are the isotopic compositions of the Eocene ocean and the ocean after ice formation, respectively. The values that were used for these variables can be found in Table 1.

The sea-water isotopic composition δ_w together with the simulated temperature T (in °C) of the four lower ocean boxes is then used to calculate the calcite isotopic composition δ_c according to the calcite-temperature relation of Shackleton (1974):

$$T = 16.9 - 4.38(\delta_c - \delta_w) + 0.1(\delta_c - \delta_w)^2 \quad (2)$$

The initial Eocene value $\delta_w{}^0$ is chosen such that the modelled Eocene deep sea temperature matches the measured late Eocene calcite isotopic composition. The prognostic equations in the model are solved using a leapfrog time scheme with a uniform time step of 6 h. All variables are averaged over 200 years (Gildor and Tziperman, 2001). For the present study biogeochemical feedback processes are ignored.

3 Results

3.1 The Eocene reference state

First the model was adapted to paleoclimatic boundary conditions representing those of the Eocene climate system. The largest differences between the climatic boundary conditions for which the model was developed (Gildor and Tziperman, 2000, 2001; Gildor et al., 2002) and those of the Eocene climate, are the position of the continents and the background atmospheric greenhouse gas concentrations. Therefore in the model the land fraction per box and pCO_2 were adjusted. Representative values for the land fractions were obtained from Markwick et al. (2000) and can be found in Table 1. A CO_2 concentration was sought for which the land ice would disappear (almost) entirely, while not (excessively) exceeding the upper-limit of 5 times PAL as set by Pagani et al. (2005).

An overview of our modelled state of the Eocene climate system at a pCO_2 of 1500 ppm is presented in Fig. 2. At this concentration, the Southern Hemispheric ice sheet has disappeared entirely, and the ice sheet in the northern box is non-perennial and a factor 10^4 smaller than it is presently (Williams and Ferrigno, 2005), see Fig. 2f. A southern sinking pattern of the MOC (Fig. 2d) was found to be a stable solution of the model for these Eocene boundary conditions. Such a state is in agreement with proxy data and model reconstructions (Thomas et al., 2003; Thomas, 2004; Via and Thomas, 2006; Coxall and Pearson, 2007).

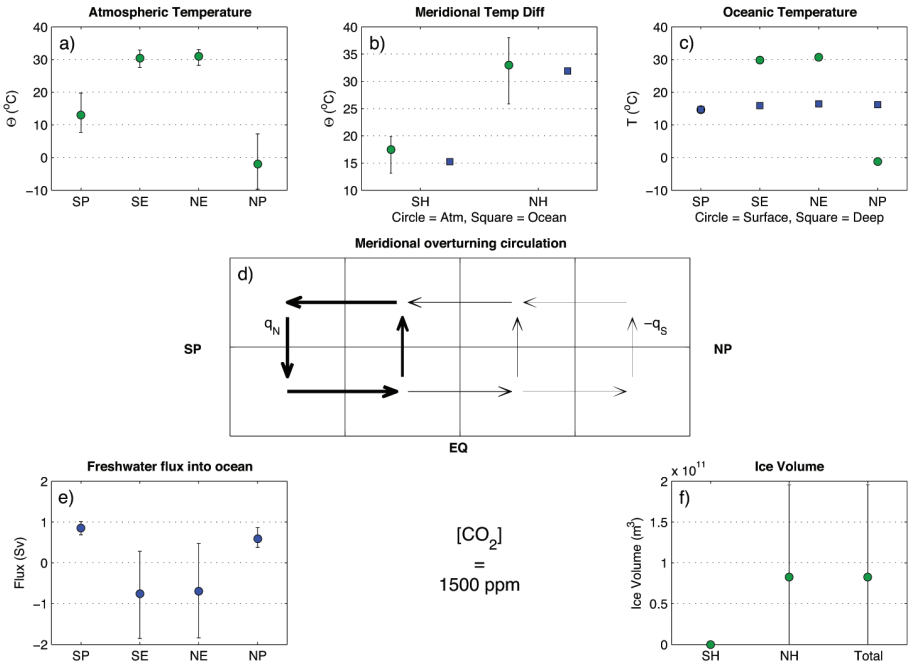

Fig. 2. Overview of the modelled state of the Eocene climate at a CO_2 concentration of 1500 ppm with the MOC in the SPP pattern; **(a)** atmospheric temperature for the southern polar (SP), southern equatorial (SE), northern equatorial (NE) and northern polar (NP) boxes; **(b)** meridional temperature difference for the Southern Hemisphere (SH) and Northern Hemisphere (NH) for the atmosphere (circles) and ocean (squares); **(c)** oceanic temperature of surface waters (circles) and deep sea (squares); **(d)** southern sinking MOC where the direction of the arrows indicates the direction of volume transport and their thickness indicates the magnitude; **(e)** freshwater flux into the ocean; **(f)** ice volume on the Southern Hemisphere (SH), Northern Hemisphere (NH) and in total; markers represent yearly averaged values, error bars indicate the seasonality.

The yearly averaged atmospheric temperature (Fig. 2a) is slightly over 30 °C in the equatorial boxes, around 13 °C in the southern box and just below freezing in the northern box. Subsequently, the atmospheric meridional temperature gradient (Fig. 2b) in the Northern Hemisphere is quite high, while taking on a more moderate value in the South. A similar pattern can be observed in the yearly averaged surface ocean temperatures (Fig. 2c). The oceanic meridional temperature gradients are therefore comparable to the atmospheric ones. In the polar boxes the seasonality is much higher (10–15 °C) than in the equatorial boxes (5 °C). The yearly averaged freshwater flux into the ocean (Fig. 2e) is positive in the polar boxes and negative in the equatorial boxes; i.e., there is evaporation at the equator and precipitation at the poles. The seasonality of the freshwater flux is much higher at the equator than at the poles.

To check the validity of this reference state, the ocean temperature results are compared with Eocene data from Bijl et al. (2009) and Liu et al. (2009), and GCM model results from Huber and Sloan (2001). In the southern and equatorial boxes, modelled SSTs are in reasonable agreement with measurements. However, proxy data as well as the GCM results indicate that both poles were relatively warm (up to 20 °C) during the Eocene. Simulated northern box temperatures are therefore too cold. Liu et al. (2009) measured deep-sea temperatures of ∼10 °C. Deep-sea temperatures in our modelled reference state are therefore too warm. Too high deep sea temperatures are a known problem of ocean box models. Values for the freshwater flux into the ocean were compared against modern-day observations (Oberhuber, 1988) and these are of the same order of magnitude, so the model determines realistic values of the buoyancy flux.

3.2 Critical threshold for continental ice formation

In order to test the hypothesis of continental ice sheet inception under a decrease of atmospheric greenhouse gas concentrations below a certain threshold value, the model was forced with a linearly decreasing CO_2 concentration. Following the measurements of Pagani et al. (2005), pCO_2 was chosen to decrease at a rate of 750 ppm per 200 kyr from 1500 ppm to 100 ppm. The carbon dioxide concentration and the corresponding Southern Hemispheric ice volume are plotted in Fig. 3a and b. The threshold CO_2 value for Antarctic ice growth is 270 ppm, at which the ice sheet starts to grow exponentially and reaches its full size within 100 kyr. Northern Hemispheric ice sheet formation begins at very low CO_2 concentrations, a result that is in qualitative agreement with the DeConto et al. (2008) model results of Cenozoic bipolar glaciation.

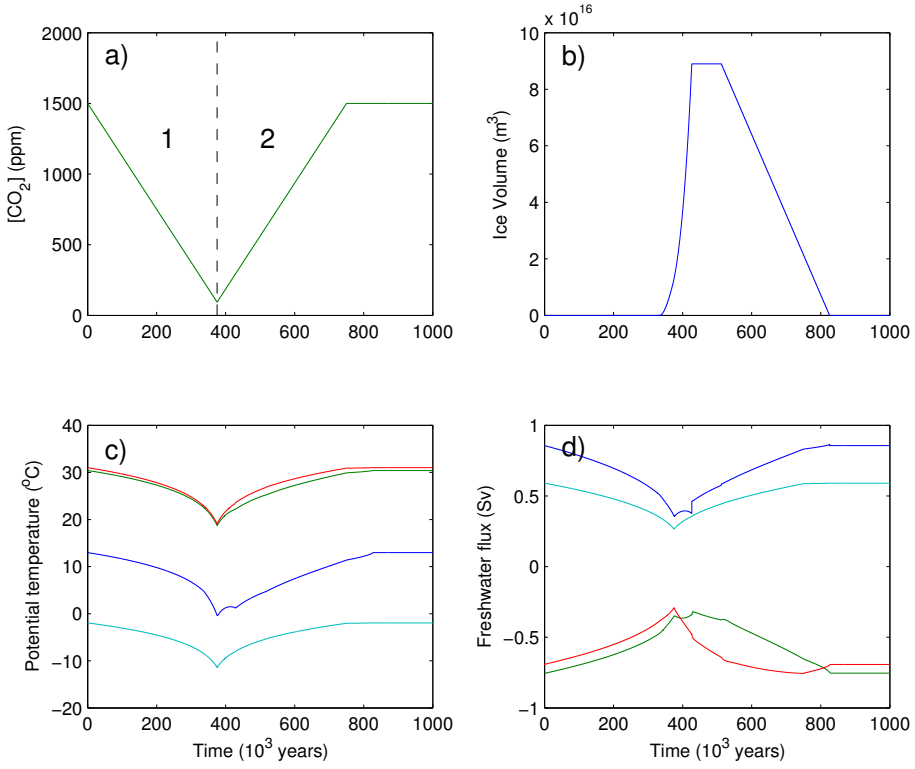

Fig. 3. Effect of **(a)** changing CO_2 concentrations on **(b)** ice volume in the southern polar box and **(c)** atmospheric temperature and **(d)** freshwater flux in the southern polar box (dark blue), southern equatorial box (green), northern equatorial box (red) and northern polar box (light blue). On the left (1 in a) is the simulation with linearly decreasing pCO_2, and on the right (2 in a) pCO_2 is raised back to its initial value and stabilises there.

The response of the climate system to decreasing carbon dioxide concentrations differs per box. At first, when no ice sheet is formed yet, the temperature decrease as plotted in Fig. 3c shows a similar pattern across the globe: slowly at first, but more rapidly as pCO_2 continues to fall. The inception of the Southern Hemispheric ice sheet lowers atmospheric temperatures in the most southern polar box and the southern equatorial box additionally through the ice-albedo feedback, while northern temperatures are barely affected. During the transition, the northern meridional temperature difference decreases, while the southern difference increases, especially after the ice sheet has started to grow. The amount of equatorial evaporation and polar precipitation decreases, see Fig. 3d.

It was also tested whether the climate system returns to its initial state when pCO_2 is raised back to 1500 ppm. The Antarctic ice sheet starts to melt at 605 ppm, a value well above the CO_2 concentration of ice inception. The difference in critical pCO_2 levels is due to the ice-albedo feedback which lowers the atmospheric temperature as long as the ice sheet is present. It takes ∼300 kyr for the ice sheet to melt entirely, and this is a linear rather than an exponential process.

Changes in temperature and freshwater flux in the northern boxes under increasing CO_2 are a mirrored version of the response to decreasing CO_2 described above: temperatures increase at a decreasing rate. The response in the southern boxes follows the melting of the Antarctic ice sheet and is therefore linear. Once the CO_2 concentration has returned to 1500 ppm and the climate system is restored to equilibrium, the global temperature and freshwater distributions are exactly the same as they were before the transition. The southern sinking state of the MOC remains unaffected throughout the transition. When the rate of pCO_2 decrease is doubled or halved the results remain qualitatively the same.

3.3 Existence of multiple climate equilibria

Differential heating of Earth's surface leads to cool, fresh polar surface waters and warm, salty equatorial surface waters. Temperature and salinity therefore have opposing roles in determining the location of deep water formation. This suggests that multiple MOC patterns are possible. This elementary problem was studied by Stommel (1961) using a density driven two-box model. It was shown that in this model indeed two different states of the MOC exist. In an extended version of this model, with three boxes (Welander, 1986; Thual and McWilliams, 1992), four solutions exist: sinking in the North and upwelling in the South (NPP), sinking in the South and upwelling in the North (SPP), sinking at both

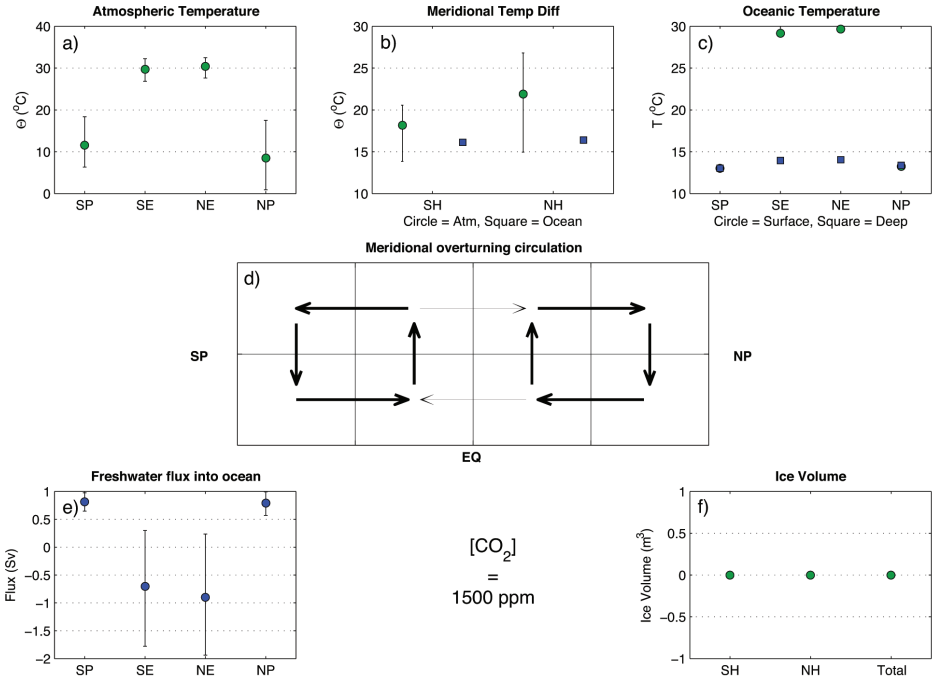

Fig. 4. Overview of the modelled state of the Eocene climate at a CO_2 concentration of 1500 ppm with the MOC in the TH pattern; **(a)** atmospheric temperature for the southern polar (SP), southern equatorial (SE), northern equatorial (NE) and northern polar (NP) boxes; **(b)** meridional temperature difference for the Southern Hemisphere (SH) and Northern Hemisphere (NH) for the atmosphere (circles) and ocean (squares); **(c)** oceanic temperature of surface waters (circles) and deep sea (squares); **(d)** bipolar sinking MOC where the direction of the arrows indicates the direction of volume transport and their thickness indicates the magnitude; **(e)** freshwater flux into the ocean; **(f)** ice volume on the Southern Hemisphere (SH), Northern Hemisphere (NH) and in total; markers represent yearly averaged values, error bars indicate the seasonality.

poles (TH), and upwelling at both poles (SA). Whether the solutions are stable depends on the boundary conditions (i.e. parameter settings) of the model. Since our ocean model is similar to the models just described, it is expected that multiple steady state solutions might exist in our Eocene climate. Indeed, for the Eocene boundary conditions a TH state (Fig. 4d) and NPP state (Fig. 5d) are also found to be stable solutions of the model, in addition to the SPP state found earlier (Fig. 2d).

The state of the MOC affects the global temperature distribution: compare Fig. 2 to Figs. 4 and 5. In the NPP and TH states there is more oceanic heat transport towards the North than in the SPP state; consequently, northern atmospheric and sea surface temperatures are higher, leading to the disappearance of the Arctic ice sheet. Northerly SSTs are in these states more in accordance with the Bijl et al. (2009) and Liu et al. (2009) data and Huber and Sloan (2001) GCM results. Similarly, southern atmospheric and sea surface temperatures in the NPP state are lower as a result of a decrease in heat transport. This lowering is insufficient to initiate the growth of an Antarctic ice sheet. Deep sea temperatures are coldest in the TH state (13.6 °C, Fig. 4c) and warmest in the NPP state (17.2 °C, Fig. 5c).

The simulations with changing pCO_2 (Sect. 3.2) showed that even if global atmospheric temperatures change drastically, the SPP state of the Eocene reference state persists. To investigate the stability of all the MOC states under decreasing CO_2 concentrations, the model was run for each state with pCO_2 decreasing with 100 ppm increments. For every CO_2 concentration the model was run until the system was in equilibrium. The pattern and strength of the MOC can be deduced from the value of $q_N - q_S$, where q_N (q_S) is the volume transport from the surface layer to the deep ocean in the northern (southern) box (Fig. 2d). A $q_N - q_S$ that is positive indicates a NPP state, a negative $q_N - q_S$ indicates a SPP state and if $q_N - q_S$ is approximately zero the ocean is in a TH state. In Fig. 6a $q_N - q_S$ is plotted against atmospheric CO_2 concentration. This bifurcation diagram shows that the SPP and the TH state of the overturning circulation coexist for all values of pCO_2. This is not the case for the NPP state, which ceases to exist for CO_2 concentrations lower than 1400 ppm. At these lower concentrations the NPP state can no longer be sustained due to a strengthening of the freshwater input into the northern polar box.

Ice formation on the Southern Hemisphere in the TH state occurs at a CO_2 concentration of 300 ppm; for the SPP state ice formation starts at 200 ppm. For concentrations lower than 100 ppm oceanic temperatures become unphysical, causing the overturning circulation to collapse into the SA state.

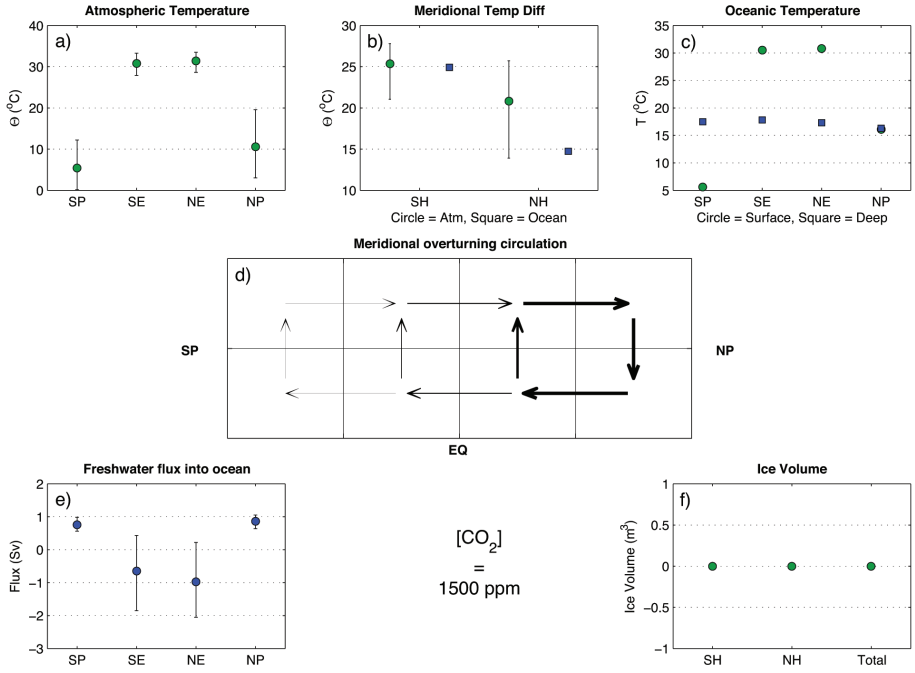

Fig. 5. Overview of the modelled state of the Eocene climate at a CO_2 concentration of 1500 ppm with the MOC in the NPP pattern; **(a)** atmospheric temperature for the southern polar (SP), southern equatorial (SE), northern equatorial (NE) and northern polar (NP) boxes; **(b)** meridional temperature difference for the Southern Hemisphere (SH) and Northern Hemisphere (NH) for the atmosphere (circles) and ocean (squares); **(c)** oceanic temperature of surface waters (circles) and deep sea (squares); **(d)** northern sinking MOC where the direction of the arrows indicates the direction of volume transport and their thickness indicates the magnitude; **(e)** freshwater flux into the ocean; **(f)** ice volume on the Southern Hemisphere (SH), Northern Hemisphere (NH) and in total; markers represent yearly averaged values, error bars indicate the seasonality.

3.4 Transitions between equilibria

The fact that the SPP and TH states coexist for the entire range of CO_2 concentrations between 100 and 1500 ppm indicates that it is possible for the climate system to switch between these states. Such a shift would be in accordance with data that show that the MOC at the E-O boundary changed from a Southern Ocean to a bipolar source of deep-water formation (Thomas et al., 2003; Thomas, 2004; Via and Thomas, 2006; Coxall and Pearson, 2007). Therefore it is tested whether it is possible to initiate such a transition in the model.

A transition from the SPP state to the TH state is induced at a CO_2 concentration of 800 ppm by adding a density perturbation to the surface layer in the northern polar box. This perturbation lasts for a short time (200 year, i.e. one averaging time-step) and is of small magnitude (1 kg m^{-3}) compared to the background density. The immediate result is that water in this box starts to sink. Subsequently, heavier water dominating the artificial perturbation is advected and causes the MOC to change to the TH state. When the CO_2 concentration is lowered further, the system remains on the TH branch (Fig. 6a). The ability of the system to switch between MOC states exists for all CO_2 concentrations. Transitions between MOC states as a result of a finite amplitude density perturbation therefore can always occur due to noise in the climate system.

The corresponding $\delta^{18}O$ profile (Fig. 6b) consists of two rapid increases, separated by a plateau. The first of these shifts represents the transition in the MOC from the SPP to the TH state. Deep sea temperatures in the TH state are colder than in the SPP state (compare Fig. 4c to 2c), because polar surface waters are colder in the North than in the South. At colder temperatures, the calcite $\delta^{18}O$ value (δ_c) is higher. During the shift, the modelled increase in $\delta^{18}O$ is 0.67‰, which corresponds to a deep sea temperature decrease of 2.8 °C. This is in accordance with the temperature decrease found by Liu et al. (2009). The second step represents Southern Hemispheric ice growth. The length of the plateau depends on the timing of the density perturbation with respect to the critical value of pCO_2 for Antarctic ice formation. As long as the pCO_2 of the MOC transition is higher than the pCO_2 of Southern Hemispheric ice inception, the $\delta^{18}O$ profile associated with a decreasing CO_2 concentration will always display a two-step signature. The magnitude of the second $\delta^{18}O$ shift is 1.22‰, of which 0.62‰ is due to ice growth. The combined magnitude of the modelled steps (1.89‰) is slightly larger than the observed 1.2–1.5‰ total increase in $\delta^{18}O$ across the E-O boundary.

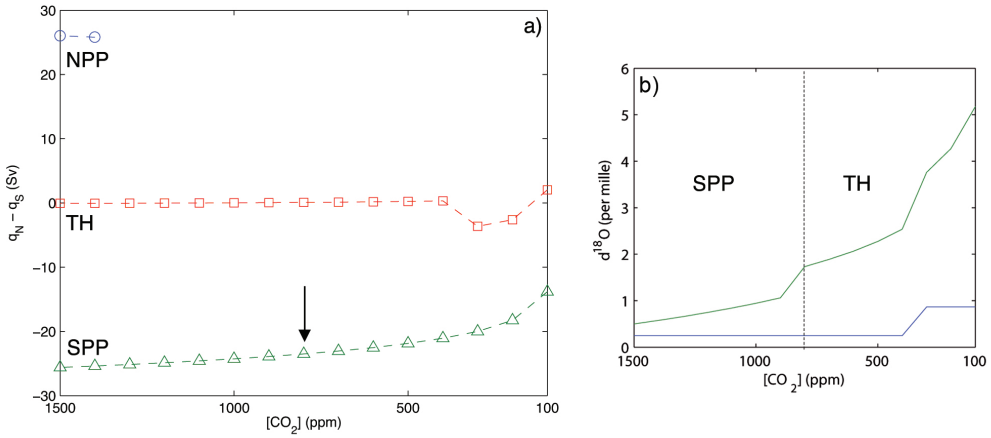

Fig. 6. (a) Simulated bifurcation diagram showing pattern and strength of the MOC for different initial states: NPP (circles), TH (squares) and SPP (triangles). The arrow denotes the CO_2 concentration at which the small density perturbation in the northern surface box was applied. **(b)** Simulated $\delta^{18}O$ profile when a density perturbation is applied to the SPP MOC in the northern surface box at a CO_2 concentration of 800 ppm. The $\delta^{18}O$ profile is separated into the contribution due to changes in ice volume (δ_w, blue) and the total signal with the added effect of deep sea temperature changes (δ_c, green). The first shift in δ_c represents the transition in the MOC from the SPP to the TH state, the second shift represents Antarctic ice growth.

Inception of ice growth on the Southern Hemisphere in our model occurs at CO_2 concentrations below 400 ppm. This is very low compared to the measurements of Pearson et al. (2009) and model studies by DeConto and Pollard (2003a,b), who estimated Antarctic ice growth to start at 750 ppm. A possible explanation for the relatively low CO_2 concentration of ice inception in the model is that the ice sheet only grows if the temperature in the polar *box* rather than *at* the pole is below 0 °C. Since the box temperature is an average, it will already be far below freezing at the pole when this threshold is reached. Therefore, the pCO_2 of ice inception might be raised by increasing the inception temperature of ice in the model.

The first test was done by raising the inception temperature of ice to 3 °C. Ice growth now occurs for CO_2 concentrations lower than 800 ppm. It is again possible to initiate a transition from the SPP to the TH state by perturbing the density. This can be done at any $pCO_2 \geq 800$ ppm; here we chose to place the perturbation at 1000 ppm. The resulting bifurcation diagram is shown in Fig. 7a. Again, the $\delta^{18}O$ shift (Fig. 7b) exhibits a two-step profile. Both steps are slightly smaller than the steps in Fig. 6b. These results show that it is indeed possible to improve the pCO_2 of ice inception in the model.

When the inception temperature is raised even higher, to 5 °C, the Eocene reference state with the MOC in the SPP pattern ceases to exist. Therefore there must exist an inception temperature between 3 and 5 °C for which the SPP state ceases to exist at a CO_2 concentration lower than 1500 ppm and higher than the pCO_2 of Antarctic ice inception. For this inception temperature, the transition from the SPP to the TH state – and hence the two-step $\delta^{18}O$ profile – will spontaneously occur in the model.

4 Summary and discussion

Global cooling and the initiation of the Antarctic ice sheet at the E-O boundary 33.7 Ma are thought to be the result of decreasing atmospheric carbon dioxide levels below a certain threshold value. Thus far, the remarkable two-step profile of the $\delta^{18}O$ record at this boundary has remained unexplained. For the late Eocene, proxy data indicate a southern sinking state of the meridional overturning circulation (MOC). Deep water formation in the northern high latitudes of the Atlantic Ocean as it is formed in the modern climate may have been initiated in the early Oligocene, possibly facilitated by tectonic changes such as the subsidence of the Greenland-Scotland Ridge (Davies et al., 2001). The role of MOC changes during the E-O climate transition has not yet been investigated. Therefore an adapted version of the simple coupled 8-box-ocean, 4-box-atmosphere model with added land ice component by Gildor and Tziperman (2000, 2001) and Gildor et al. (2002) was used to simulate the response of the full climate system to a decrease in pCO_2.

First the Eocene reference state was found by changing the land fractions in the model and raising the CO_2 concentration to 1500 ppm. The MOC displayed a southern sinking (SPP) state, in accordance with proxy data. Under these boundary conditions, a northern sinking (NPP) and bipolar sinking (TH) state are also stable solutions. When the model is forced with decreasing pCO_2 it naturally becomes colder. At low carbon dioxide concentrations (270 ppm) an Antarctic ice sheet is formed. The SPP state of the MOC remains unaffected by the climatic changes. Therefore it was tested whether all states of the MOC exist for all CO_2 concentrations lower than 1500 ppm.

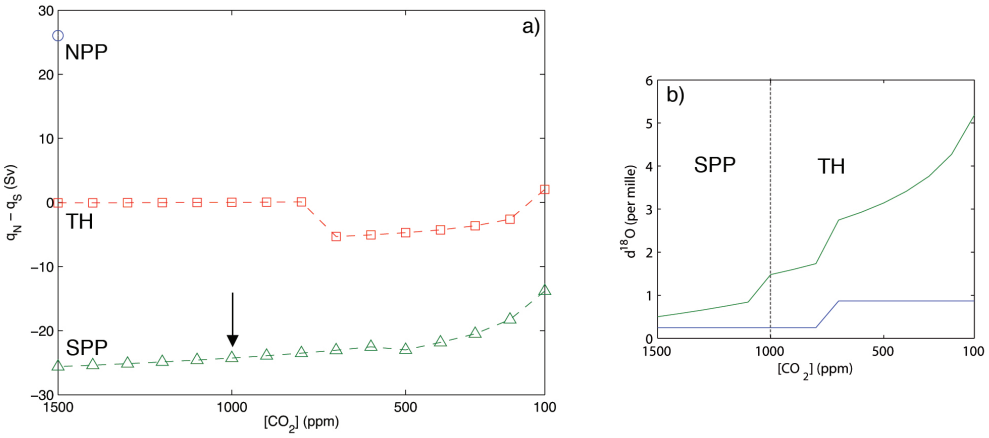

Fig. 7. Same as Fig. 6 but with the inception temperature of ice increased to 3 °C: **(a)** Simulated bifurcation diagram showing pattern and strength of the MOC for different initial states: NPP (circles), TH (squares) and SPP (triangles). The arrow denotes the CO_2 concentration at which the small density perturbation in the northern surface box was applied. **(b)** Simulated $\delta^{18}O$ profile when a density perturbation is applied to the SPP MOC in the northern surface box at a CO_2 concentration of 1000 ppm. The $\delta^{18}O$ profile is separated into the contribution due to changes in ice volume (δ_w, blue) and the total signal with the added effect of deep sea temperature changes (δ_c, green). The first shift in δ_c represents the transition in the MOC from the SPP to the TH state, the second shift represents Antarctic ice growth.

The NPP state ceases to exist for CO_2 concentrations lower than 1400 ppm. Both the SPP and the TH pattern exist for all levels of pCO_2 between 100 and 1500 ppm. This suggests that it is possible for the system to switch between these MOC states. The switch in overturning state leads to a cooling of the deep sea and hence a positive excursion of $\delta^{18}O$ values. The second step in the $\delta^{18}O$ record can be interpreted as representing the rapid glaciation of the Antarctic ice sheet.

In our model, a transition from the SPP to the TH state was induced by means of a small density perturbation. In reality, a switch between different MOC states may be induced by various mechanisms: given the small value of the density perturbation necessary to induce the MOC transition, it may be induced by (random) fluctuations in the strength of the hydrological cycle. Alternatively, tectonic changes, which have not been considered here, may initiate or at least help to establish another MOC pattern. In particular, two tectonic events have been timed around the E-O boundary, which may have facilitated a transition to NH deep water formation:

i. The subsidence of the Greenland-Scotland Ridge may have facilitated North Atlantic deep water formation (Davies et al., 2001; Abelson et al., 2008).

ii. The possible development of an unrestricted (but most likely still very shallow) Antarctic circumpolar zonal flow by the opening of the Tasman Gateway and Drake Passage around the E-O boundary may decrease the strength of Southern Hemisphere deep water formation via the geostrophic balance and in turn facilitate Northern Hemisphere deep water formation. Many previous modeling studies have shown that Southern Ocean deep water formation is reduced when there exists an unrestricted zonal circum-Antarctic flow (Mikolajewicz et al., 1993; Toggweiler and Samuels, 1995); this effect is often referred to as the "Drake Passage effect". In Dijkstra et al. (2003) the different Atlantic MOC states were investigated in a three dimensional ocean model with an open and closed southern channel. In that study the "Drake Passage effect" leads to a preference of a state with northern sinking when opening the southern channel (see their Fig. 5). When considering the temperature change due to the establishment of an Antarctic circumpolar flow, the Southern Ocean SSTs cool, while the northern hemispheric SSTs warm (Toggweiler and Bjornsson, 2000; Nong et al., 2000; Sijp and England, 2004). In view of the study by Dijkstra et al. (2003) at least part of the Southern Ocean cooling is due to a transition from one MOC state with more southern deep water formation to one with more northern deep water formation. The opening of Drake Passage and the establishment of a first (weak) Antarctic Circumpolar Current could therefore have induced the SPP to TH transition (as accomplished in our box model by a (small) density perturbation) because of the preference for northern sinking.

While the opening of gateways may have helped to induce a transition in the MOC pattern, the timing of these gateway changes remains controversial. It is therefore interesting to repeat here that in our model a very small density perturbation is enough to induce the transition.

The CO_2 concentration of ice inception was increased by increasing the inception temperature of ice in the model. At

an inception temperature of 3 °C (averaged over the entire southern polar box) ice growth is initiated below 800 ppm. This is in close agreement with data and modelling studies. For an ice inception temperature of 5 °C, the Eocene reference state with the MOC in a SPP pattern ceases to exist. This suggests that an inception temperature between 3 and 5 °C exists for which the transition from the SPP to the TH state under decreasing pCO_2 occurs spontaneously.

Despite the fact that a model of very low complexity was used to simulate the Eocene-Oligocene transition, our new interpretation of the $\delta^{18}O$ record appears to be coherent and complies qualitatively well with proxy data. Quantitative model-data comparisons, however, are difficult in this context and should be done with caution. Due to the model's simplistic representation of radiative transfer, model CO_2 should be thought of as only representing rough changes in radiative forcing. The exact values of the threshold CO_2 concentrations for ice formation as found in DeConto and Pollard (2003a,b) and DeConto et al. (2008) model studies can therefore not directly be compared as they depend on model parameters. The same holds for CO_2 reconstructions (Pagani et al., 2005; Pearson et al., 2009), which themselves contain large uncertainties.

The exact timing of the modelled shifts and intermittent plateau is still undetermined and is largely dependent on the exact pattern of pCO_2 change. The total magnitude of the two modelled steps is slightly larger than the estimates from $\delta^{18}O$ proxy records. This can be attributed to the second step – representing Antarctic ice growth – being overestimated. In our model simulations, the Southern Hemispheric ice sheet was allowed to grow to its full size, $2.57 \times 10^{16}\,m^3$, the present-day size of the Antarctic ice sheet. This is on the high end of the maximum E-O ice volume estimates (40–120% of modern Antarctic ice volume, Liu et al., 2009). It takes the ice sheet ∼100 kyr to grow to this size, while data indicate that the second step only lasted for 40 kyr. Therefore there must have been a mechanism that stopped the growth of the Antarctic ice sheet after 40 kyr. This mechanism might be related to the CO_2 record, which is known to have displayed variable rates of changes around the E-O boundary. According to measurements by Pearson et al. (2009), there might even have been a temporary increase in CO_2 concentrations during the second step, which could have stabilised the growth of the ice sheet.

Northern polar temperatures in our modelled Eocene reference state were found to be too cold, and deep sea temperatures were found to be too warm. These discrepancies between modelled temperatures and data are a shortcoming of the model. The too cold Northern polar temperatures in our model can be attributed to the lack of Northern Hemispheric deep water formation and consequently reduced oceanic heat transport to northern high latitudes. The box model does not include the wind-driven ocean circulation, which is partially responsible for oceanic meridional heat transport, so meridional heat transport differences due to the locations of deep water formation are overestimated. In a more realistic model, the temperature difference between northern and southern high latitudes in a southern sinking pattern of the MOC would therefore be less severe. The data of Liu et al. (2009) do suggest slightly colder Northern Hemisphere SSTs than in the Southern Hemisphere *before* the E-O transition. Furthermore, an increased seasonality in northern high latitudes before the Oi-1 event as suggested by Eldrett et al. (2009) would also support relatively cool NH winter SSTs.

Although changes in MOC and ice volume under decreasing CO_2 concentrations prove to be a plausible explanation for the observed $\delta^{18}O$ signal, possible mechanisms behind the pCO_2 decline remain unaddressed. In our model study atmospheric pCO_2 was a prescribed forcing and not an output variable. Proposed causes of the CO_2 decline in the literature are reduced sea-floor spreading, increased silicate weathering, increased marine production and release of organic carbon from geological reservoirs (Zachos and Kump, 2005; Coxall and Pearson, 2007; Pearson et al., 2009). Positive feedback mechanisms exist between these processes and the changes in MOC and ice volume found in our simulations. The role and strength of these mechanisms could be tested with the biogeochemical module developed by Gildor et al. (2002) or the more comprehensive models of Zachos and Kump (2005) and Merico et al. (2008), but are outside the scope of this paper.

In this model study, only a limited number of feedback processes has been incorporated. These processes have proven to be sufficient to newly interpret the $\delta^{18}O$ record at the E-O boundary. Nonetheless, the results of this research will be even more robust when they can be reproduced using more complex models. The role of several potentially important processes should be investigated in the future. To fully understand the influence of the opening of oceanic gateways, a full three-dimensional ocean model should be used in which (i) Southern Ocean dynamics are included and an ACC can be formed, (ii) separate Atlantic and Pacific ocean basins are included with varying connections between them, and (iii) the dynamics of the overflow at the Greenland-Scotland ridge is accounted for. It will also be interesting to see how the changes described here affect atmospheric circulation patterns, and vice versa. Although the land ice module used in this study is very simple, its results are in qualitative agreement with those in DeConto and Pollard (2003a,b). Of course, the precise details of Antarctic ice sheet formation can be better understood from their simulations. Changes in orbital configuration were not taken into account in our simulations, even though they are thought to have played a significant role.

This model study has provided us with a new mechanism for the two-step $\delta^{18}O$ profile at the E-O boundary. It was found that the first step is the result of a transition in the ocean's MOC from a southern to a bipolar sinking state. This transition leads to a cooling of the deep sea and thus to an increase in marine benthic $\delta^{18}O$ values. The second

step represents rapid Antarctic ice growth, caused by lowering of the atmospheric carbon dioxide levels below a certain threshold level. The two-step signature will always occur when the MOC transition – which can occur spontaneously due to random density perturbations or can be induced by tectonic changes – occurs at higher pCO_2 levels than the critical pCO_2 level for Southern Hemispheric ice formation. The mechanisms that are proposed here are qualitatively in close agreement with proxy data, and so is the order of magnitude of the two modelled $\delta^{18}O$ steps.

Acknowledgements. We thank Hezi Gildor for kindly providing us with the model used in this study and helping us with the set-up. We also thank Helen Coxall and Dorian Abbot for their constructive and insightful reviews, the Editor for valuable comments, and Bas de Boer and Roderik van de Wal for fruitful discussions.

Edited by: G. Lohmann

References

Abelson, M., Agnon, A., and Almogi-Labin, A.: Indications for control of the Iceland plume on the Eocene-Oligocene "greenhouse-icehouse" climate transition, Earth Planet. Sci. Lett., 265, 33–48, 2008.

Bijl, P. K., Schouten, S., Sluijs, A., Reichart, G.-J., Zachos, J. C., and Brinkhuis, H.: Early Palaeogene temperature evolution of the Southwest Pacific Ocean, Nature, 461, 776–779, 2009.

Bintanja, R., van de Wal, R. S. W., and Oerlemans, J.: Modelled atmospheric temperatures and global sea levels over the past million years, Nature, 437, 125–128, 2005.

Coxall, H. K. and Pearson, P. N.: The Eocene-Oligocene Transition, in: Deep-Time Perspectives on Climate Change: Marrying the Signal from Computer Models and Biological Proxies, edited by: Williams, M., Haywood, A. M., Gregory, F. J., and Schmidt, D. N., 351–387, The Micropalaeontological Society Special Publication, 2007.

Coxall, H. K., Wilson, P. A., Pälike, H., Lear, C. H., and Backman, J.: Rapid stepwise onset of Artarctic glaciation and deeper calcite compensation in the Pacific Ocean, Nature, 433, 53–57, 2005.

Cramer, B. S., Toggweiler, J. R., Wright, J. D., Katz, M. E., and Miller, K. G.: Ocean overturning since the Late Cretaceous: Inferences from a new benthic foraminiferal isotope compilation, Paleoceanography, 24, PA4216, doi:10.1029/2008PA001683, 2009.

Davies, R., Cartwright, J., Pike, J., and Line, C.: Early Oligocene Initiation of North Atlantic Deep Water Formation, Nature, 410, 917–920, 2001.

de Boer, B., van de Wal, R., Bintanja, R., Lourens, L., and Tuenter, E.: Cenozoic global ice-volume and temperature simulations with 1-D ice-sheet models forced by benthic $\delta^{18}O$ records, Annals of Glaciology, 51, 23–33, 2010.

DeConto, R. M. and Pollard, D.: Rapid Cenozoic glaciation of Antarctica induced by declining atmospheric CO_2, Nature, 421, 245–249, 2003a.

DeConto, R. M. and Pollard, D.: A coupled climate-ice sheet modeling approach to the Early Cenozoic history of the Antarctic ice sheet, Palaeogeogr. Palaeocl., 198, 39–52, 2003b.

DeConto, R. M., Pollard, D., Wilson, P. A., Pälike, H., Lear, C. H. and Pagani, M.: Thresholds for Cenozoic bipolar glaciation, Nature, 455, 652–656, 2008.

Dijkstra, H. A., Weijer, W., and Neelin, J. D.: Imperfections of the three-dimensional thermohaline ocean circulation: Hysteresis and unique state regimes, J. Phys. Oceanogr., 33, 2796–2814, 2003.

Dockery, D. and Lozouet, P.: Biotic patterns in Eocene-Oligocene Molluscs of the Atlantic Coastal Plain, USA, in: From Greenhouse to Icehouse, edited by: Prothero, D. R., Ivany, L., and Nesbitt, E. A., 303–340, Columbia University Press, 2003.

Eldrett, J. S., Harding, I. C., Wilson, P. A., Butler, E., and Roberts, A. P.: Continental ice in Greenland during the Eocene and Oligocene, Nature, 446, 176–179, 2007.

Eldrett, J. S., Greenwood, D. R., Harding, I. C., and Huber, M.: Increased seasonality through the Eocene to Oligocene transition in northern high latitudes, Nature, 459, 969–974, doi:10.1038/nature08069, 2009.

Ghil, M., Mulhaupt, A., and Pestiaux, P.: Deep water formation and Quaternary glaciations, Clim. Dyn., 2, 1–10, 1987.

Gildor, H. and Tziperman, E.: Sea ice as the glacial cycles' climate switch: role of seasonal and orbital forcing, Paleoceanography, 15, 605–615, 2000.

Gildor, H. and Tziperman, E.: A sea ice climate switch mechanism for the 100-kyr glacial cycles, J. Geophys. Res., 106, 9117–9133, 2001.

Gildor, H., Tziperman, E., and Toggweiler, J.: Sea ice switch mechanism and glacial-interglacial CO_2 variations, Global Biogeochem. Cy., 16, GB0203, doi:10.1029/2001GB001446, 2002.

Hay, W. W., Flögel, S., and Söding, E.: Is the initiation of glaciation on Antarctica related to a change in the structure of the ocean?, Global Planet. Change, 45, 23–33, 2005.

Haywood, A., Valdes, P., Lunt, D., and Pekar, S.: The Eocene-Oligocene boundary and the Antarctic Circumpolar Current, in: Geophysical Research Abstracts, vol. 12, pp. EGU2010–5031, 2010.

Huber, M. and Nof, D.: The ocean circulation in the southern hemisphere and its climate impacts in the Eocene, Palaeogeogr. Palaeocl., 231, 9–28, 2006.

Huber, M. and Sloan, L. C.: Heat transport, deep waters, and thermal gradients: coupled simulation of an Eocene greenhouse climate, Geophys. Res. Lett., 28, 3481–3484, 2001.

IPCC: Climate Change 2007: the Physical Science Basis. Contribution of Working Group I to the Fourth Assessment Report of the Intergovernmental Panel on Climate Change, Cambridge University Press, Cambridge, United Kingdom and New York, NY, USA, 2007.

Lear, C. H., Elderfield, H., and Wilson, P. A.: Cenozoic deep-sea temperatures and global ice volumes from Mg/Ca in benthic foraminiferal calcite, Science, 287, 269–272, 2000.

Lear, C. H., Rosenthal, Y., Coxall, H. K., and Wilson, P. A.: Late Eocene to early Miocene ice-sheet dynamics and the global carbon cycle, Paleoceanography, 19, PA4015, doi:10.1029/2004PA001039, 2004.

Lear, C. H., Bailey, T. R., Pearson, P. N., Coxall, H. K., and Rosenthal, Y.: Cooling and ice growth across the Eocene-Oligocene

transition, Geology, 36, 251–254, 2008.
Liu, Z., Pagani, M., Zinniker, D., DeConto, R., Huber, M., Brinkhuis, H., Shah, S. R., Leckie, R. M., and Pearson, A.: Global cooling during the Eocene-Oligocene climate transition, Science, 323, 1187–1190, 2009.
Livermore, R., Nankivell, A., Eagles, G., and Morris, P.: Paleogene opening of Drake passage, Earth Planet. Sc. Lett., 236, 459–470, 2005.
Markwick, P. J., Rowley, D. B., Ziegler, A. M., Hulver, M. L., Valdes, P. J., and Sellwood, B. W.: Late Cretaceous and Cenozoic global palaeogeographies: Mapping the transition from a "hot-house" to an "ice-house" world, GFF, 122, p. 103, 2000.
Merico, A., Tyrrell, T., and Wilson, P. A.: Eocene/Oligocene ocean de-acidification linked to Antarctic glaciation by sea-level fall, Nature, 452, 979–982, 2008.
Mikolajewicz, U., Maier-Reimer, E., Crowley, T., and Kim, K.: Effects of Drake and Panamanian Gateways on the circulation of an ocean model, Paleoceanograpy, 8, 409–426, 1993.
Nong, G. T., Najjar, R. G., Seidov, D., and Peterson, W. H.: Simulation of Ocean Temperature Change due to the Opening of Drake Passage, Geophys. Res. Lett., 27, 2689–2692, 2000.
Oberhuber, J. M.: An atlas based on "COADS" data set, Tech. Rep. 15, Max-Planck-Institut für Meteorologie, 1988.
Oerlemans, J.: Correcting the δ^{18}O deep-sea temperature record for Antarctic ice volume, Palaeogeogr. Palaeocl., 208, 195–205, 2004.
Pagani, M., Zachos, J. C., Freeman, K. H., Tipple, B., and Bohaty, S.: Marked decline in atmospheric carbon dioxide concentrations during the paleogene, Science, 309, 600–603, 2005.
Pearson, P. N., Foster, G. L., and Wade, B. S.: Atmospheric carbon dioxide through the Eocene-Oligocene climate transition, Nature, 461, 1110–1113, 2009.
Rea, D. K. and Lyle, M. W.: Paleogene calcite compensation depth in the eastern subtropical Pacific: answers and questions, Paleoceanography, 20, PA1012, doi:10.1029/2004PA001064, 2005.
Scher, H. D. and Martin, E. E.: Timing and climatic consequences of the opening of Drake passage, Science, 312, 428–430, 2006.
Shackleton, N. J.: Attainment of isotopic equilibrium between ocean water and the benthonic foraminifera genus Uvigerina: isotopic changes in the ocean during the last glacial, C. N. R. S. Colloq., 219, 203–209, 1974.
Sijp, W. P., England, M. H., and Toggweiler, J. R.: Effect of Ocean Gateway Changes under Greenhouse Warmth, J. Climate, 22, 6639–6652, doi:10.1175/2009JCLI3003.1, 2009.
Sijp, W. and England, M.: Effect of the Drake Passage throughflow on global climate, J. Phys. Oceanogr., 34, 1254–1266, 2004.
Stommel, H.: Thermohaline convection with two stable regimes of flow, Tellus, 13, 224–230, 1961.
Thomas, D. J.: Evidence for deep-water production in the North Pacific Ocean during the early Cenozoic warm interval, Nature, 430, 65–68, 2004.
Thomas, D. J., Bralower, T. J., and Jones, C. E.: Neodymium isotopic reconstruction of late Paleocene-early Eocene thermohaline circulation, Earth Planet. Sc. Lett., 209, 309–322, 2003.
Thual, O. and McWilliams, J. C.: The catastrophe structure of thermohaline convection in a two-dimensional fluid model and a comparison with low-order box models, Geophys. Astro. Fluid, 64, 67–95, 1992.
Toggweiler, J. R. and Bjornsson, H.: Drake Passage and Paleoclimate, J. Quat. Sci., 15, 319–328, 2000.
Toggweiler, J. R. and Samuels, B.: Effect of Drake Passage on the global thermohaline circulation, Deep-Sea Res., 42, 477–500, 1995.
Via, R. K. and Thomas, D. J.: Evolution of Atlantic thermohaline circulation: Early Oligocene onset of deep-water production in the North Atlantic, Geology, 34, 441–444, 2006.
Welander, P.: Thermohaline effects in the ocean circulation and related simple models, in: Large-Scale Transport Processes in Oceans and Atmosphere, edited by: Willebrand, J. and Anderson, D. L. T., 163–200, D. Reidel, 1986.
Williams, Jr., R. S. and Ferrigno, J. G.: Satellite Image Atlas of Glaciers of the World, USGS Fact Sheet 2005–3056, 2005.
Zachos, J. C. and Kump, L. R.: Carbon cycle feedbacks and the initiation of Antarctic glaciation in the earliest Oligocene, Global Planet. Change, 47, 51–66, 2005.
Zachos, J. C., Quinn, T. M., and Salamy, K. A.: High-resolution (10^4 years) deep-sea foraminiferal stable isotope records of the Eocene-Oligocene climate transition, Paleoceanography, 11, 251–266, 1996.